J Mater Sci (2014) 49:2773–2780
DOI 10.1007/s10853-013-7980-7

Effects of grain refinement and disorder on the electronic properties of nanocrystalline NiO

G. Domínguez-Cañizares · A. Gutiérrez · J. Chaboy · D. Díaz-Fernández · G. R. Castro · L. Soriano

Received: 16 August 2013 / Accepted: 18 December 2013 / Published online: 7 January 2014

Abstract Nanocrystalline NiO thin films have been grown on different substrates by RF magnetron sputtering with mixed O_2-Ar plasma composition. The oxygen content of the plasma was varied between 0 and 100 %. The films were characterized by scanning electron microscopy (SEM), X-ray diffraction (XRD), X-ray photoelectron spectroscopy (XPS), and extended X-ray absorption fine structure (EXAFS). SEM results reveal a grain refinement when oxygen is added to the plasma. This effect can also be observed by XRD, where an analysis of the peak width confirms this decrease in the grain size. The analysis of EXAFS data shows that the presence of O_2 in the plasma induces lattice disorder, as evidenced by the observed increase of the Debye–Waller factor. These microstructural changes modify the electronic structure of the NiO thin films. The spectral line shape in Ni 2*p* XPS spectra shows clear differences between samples grown with and without O_2 in the plasma. These differences can be explained in terms of the observed structural changes.

G. Domínguez-Cañizares · A. Gutiérrez (✉) · D. Díaz-Fernández · L. Soriano
Departamento de Física Aplicada & Instituto de Ciencia de Materiales Nicolás Cabrera, Universidad Autónoma de Madrid, Cantoblanco, 28049 Madrid, Spain
e-mail: a.gutierrez@uam.es

J. Chaboy
Departamento de Física de la Materia Condensada & Instituto de Ciencia de Materiales de Aragón (CSIC), Universidad de Zaragoza, 50009 Saragossa, Spain

G. R. Castro
SpLine CRG BM25 Beamline, European Synchrotron Radiation Facility, BP 220, 6 rue Jules Horowitz, 38043 Grenoble, France

G. R. Castro
Instituto de Ciencia de Materiales de Madrid, Sor Juana Inés de la Cruz, 3, 28049 Madrid, Spain

Introduction

Nickel oxide is an interesting technological material due to its wide range of applications, which are currently the subject of active research. For instance, NiO and $Ni_{1-x}O$ in the form of thin films have a key role in electrochemical supercapacitors [1, 2], electrochromic films [3], gas sensors [4], lithium-ion batteries [5], and different catalytic applications, such as the reduction of methane to produce hydrogen [6, 7]. In all these applications the interaction of the NiO films with the environment plays an important role. Therefore, these materials are usually grown as nanostructured films with a high surface-to-volume ratio.

From a fundamental point of view, the electronic properties of NiO have originated much debate in the last decades [8–10]. Indeed, the lineshape of the Ni 2*p* photoemission spectra is still controversial, especially the shoulder at 1.5 eV from the main peak [11]. It has been recently proposed that the intensity of this satellite is originated by non-local screening and surface effects [12]. In nanostructured NiO samples, where the surface-to-volume ratio is enhanced, this feature results to be more intense [13, 14].

Nickel oxide thin films can be grown via many deposition methods, both chemical and physical [15–17]. Among the physical deposition techniques magnetron sputtering has centered much interest due to its ability to grow coatings with a wide variety of final properties. Magnetron sputtering has been used in recent years to deposit NiO using both direct and alternate current on different substrates [18–20]. Due to the out-of-equilibrium

nature of the sputtering process the final properties of the films are highly dependent on the growing parameters: substrate temperature, sputter gas composition, magnetron power, distance and angle between substrate and target, time of deposition, and working pressure. For instance, the influence of substrate temperature and working pressure modifies the structure of the films as predicted by the structure zone model of Thornton [21]. In our case, the relevant parameter is the plasma composition. In a previous work, we obtained nanostructured NiO films with different structural and electrical properties by using different mixtures of argon and oxygen in the plasma [22]. In the present work, we show how the structural changes induced by the presence of O_2 in the sputtering plasma, especially the crystallite size and the lattice disorder, affect the electronic structure of the films observed by XPS, especially the observed differences in the surface contribution to the Ni $2p$ line shape.

Materials and methods

Nanostructured NiO thin films were grown by radio frequency magnetron sputtering of a NiO target (AJA International, 99.95 % purity). The base pressure of the vacuum chamber was in the lower 10^{-7} mbar range, and the pressure used for plasma ignition was 1.5×10^{-2} mbar. This pressure was kept constant during the whole deposition time (1 h). The plasma was composed of a mixture of oxygen and argon, with an oxygen content ranging from 0 to 70 %. Different substrates were used in order to study the effects of the substrate surface morphology on the final properties of the NiO films. Glass microscope slides and single-crystal silicon wafers [p-type with (100) orientation] were used as planar substrates. Commercial (Synkera Technologies) anodic alumina membranes (AAM) grown on aluminum were used as nanostructured substrates. The pore diameter of the AAM was $\approx$ 35 nm, and the distance between pores was $\approx$100 nm, which gives a porosity of approximately 11 % by geometrical estimation. The thickness of the AAM was 500 nm. Except for the AAM, all substrates were ultrasonically cleaned by immersing them subsequently into acetone and methanol. The substrates were rotated during deposition at about 10 rpm in order to obtain a more uniform film. The angle of the sputtering cathode with respect to the normal to the substrates surface was 23° (off-axis), and the distance between target and substrate was 8 cm. Before starting deposition a pre-sputtering of 5 min was performed in order to clean the target surface. The magnetron power was set to 100 W. Although no heating was applied, a temperature increase of about 50 °C above room temperature, induced by the plasma, was observed at the surface of the substrates at the end of the deposition, as monitored by an IR external pyrometer operating through a sapphire window.

The morphology of the deposited NiO films was observed by scanning electron microscopy (SEM), using a Philips XL30 S-FEG microscope equipped with a field-emission cathode, at an accelerating voltage of 20 kV. X-ray diffraction (XRD) measurements were carried out with a Panalytical Xpert PRO diffractometer in grazing incidence condition. In the setup used, an X-ray Cu tube with the corresponding optical setup provides a parallel and monochromatic X-ray beam. XRD data were collected with a beam incidence angle of 1° and a $2q$ scan between 30° and 70° with a step size of 0.03° and a counting time of 5 s/step. The XRD data were used to calculate the mean crystal size using the Scherrer approximation, with a confidence range of 10 %.

X-ray absorption spectra (XAS) were measured above the Ni K-edge ($E \approx$ 8.3 keV) at the SpLine BM25 experimental station of the European Synchrotron Radiation Facility (ESRF) in Grenoble, France. Measurements were carried out at room temperature in fluorescence mode, using a multi-element solid-state multichannel detector. The XAS spectra were processed according to standard procedures [23] and the corresponding extended X-ray absorption fine structure (EXAFS) was analyzed by using the VIPER program [24, 25]. Every measurement and fitting was systematically performed on samples deposited on AAM and Si substrates, with no significant differences. A NiO cluster of 6 Å, with NaCl-type structure (fcc), was simulated with the software ATOMS. Then the phase shift and backscattering amplitudes were calculated for a maximum path of 4 legs with the use of the FEFF5 code. Only the first two shells were used in the fittings, neglecting the multiple-scattering paths due to the high level of disorder of the samples. In order to obtain the EXAFS signal the data were multiplied by k^2 to compensate for the amplitude reduction at large k values. X-ray photoelectron spectroscopy (XPS) measurements were carried out using a CLAM4 electron energy analyzer and a twin anode (Mg and Al) X-ray source from Thermo-Scientific. The pass energy was set to 20 eV in order to have a good equilibrium between count rate and energy resolution.

Results

Figure 1 shows high-resolution SEM images of NiO thin films grown on nanoporous AAM templates (Fig. 1a–d) and on single-crystal Si wafers (Fig. 1e, f). Images 1a, c, and e, at the left, correspond to samples grown with pure Ar plasma, whereas images 1b, d, and f, at the right, correspond to samples grown with 70 % oxygen in the reactive plasma. As it can be seen in Fig. 1a–d, NiO thin films

keep the hexagonal structure of the AAM after deposition. This effect is independent of the oxygen content in the reactive plasma: all samples preserve the substrate pattern. However, some differences in the morphology of the deposited films can be observed between samples grown with and without oxygen in the plasma. Figure 1a reveals irregular patterns around the pores, with sharp edges and well-defined angles, suggesting a polycrystalline growth with crystals of different orientations growing independently of each other, showing up different facets in the top view image. On the other hand, Fig. 1b shows a morphology with more softened and smooth edges, resembling amorphous growth, or, at least, a considerable refinement of the crystal size. This effect can also be observed in the NiO thin films grown on flat Si substrates (Fig. 1e, f). The sample grown without oxygen in the plasma shows a fine structure, with very irregular patterns, and grain size large enough to be resolved with the current microscope setup. On the other hand, the image taken on the sample grown with 70 % oxygen in the plasma, shown in Fig. 1f, is not able to resolve the grain structure.

Figure 1c and d shows cross sections of the NiO films deposited on AAM substrates. Details of the pores and the pore walls are clearly resolved. The NiO films correspond to the upper, brighter region, which extends about one fifth of the height of the pores, which is nominally 500 nm. The thicknesses of both samples are of the same order of magnitude. According to this image, the created thin films have a columnar structure on the top of the AAM columns with the growth direction perpendicular to the surface. In every sample the pores are unblocked and the NiO thin films maintain the columnar growth surrounding the pores in a hexagonal arrangement. Note that the possibility to grow hexagonally patterned nanoporous NiO films might have significance in some technological applications, such as in magnetic exchange-bias devices or in catalytic nano reactors. Columnar growth is expected under the current conditions. According to Thornton [21], for temperatures

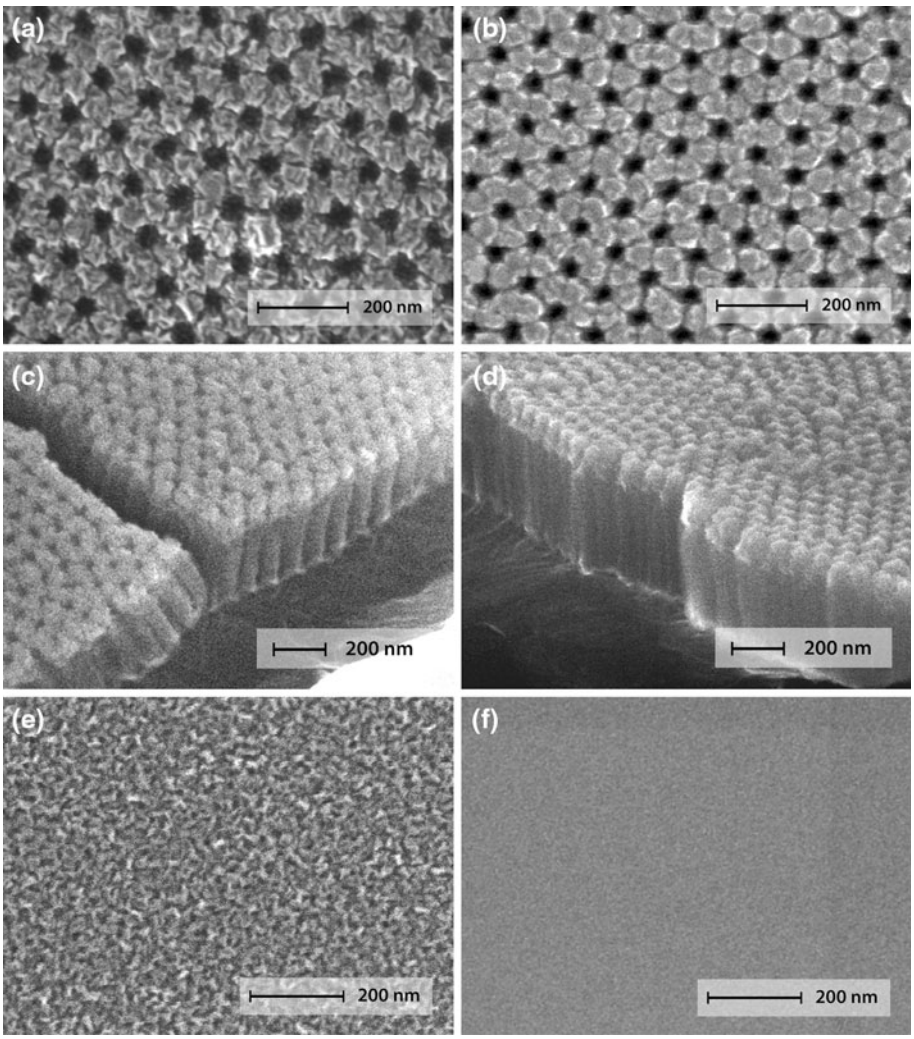

Fig. 1 NiO thin films grown on AAM substrates (**a**)–(**d**) and on Si substrates (**e**) and (**f**). The *left column* shows samples grown with no oxygen in the plasma, while the *right column* shows samples grown with 70 % oxygen content in the sputtering plasma

well below the melting point and high argon pressures there is little adatom surface mobility, and the initial nuclei tend to grow in the direction of the available coating flux.

The grain refinement shown in Fig. 1 for samples grown with oxygen in the plasma should be detected by other structural techniques, like XRD. Figure 2 shows a detail of the (100) diffraction peak for samples grown with pure argon and 70 % O_2 in the plasma, respectively. No differences were observed between samples grown on different substrates. The solid line through the data points is the result of a standard least-squares fit using a pseudo-Voigt curve. The intensity of the diffraction peak in the case of the 70 % sample is about eight times lower than that of the 0 % sample, although this difference is not appreciated in the figure because we used an arbitrary scale to plot both peaks with a similar aspect, in order to emphasize their differences in width and position. This difference in intensity is evidenced, however, by the different signal-to-noise ratio of both curves. The lower intensity of the diffraction peaks for the sample grown with oxygen suggests a lower crystal quality. Additionally, the position and width of the (100) peak of this sample differ from the values obtained for the sample grown with pure Ar. The peak is shifted towards lower Bragg angles, which indicates an expansion of the crystal lattice of about 1–2 % for samples with oxygen in the plasma. This effect is gradual, increasing with the oxygen content of the plasma, as has been reported in previous works [22, 26], and can be associated to a distortion of the lattice induced by an excess oxygen in it. Indeed, the presence of Ni vacancies in this kind of NiO thin films has been very recently reported, with a concentration that increases linearly with the oxygen content of the plasma [27].

The width of the diffraction peaks can be associated to the mean crystal size in nanocrystalline materials: the larger the width, the smaller the crystal size. The larger width observed for the 70 % sample as compared with the sample grown with pure Ar indicates that the mean size of NiO grains in the former case is smaller than in the latter one. Both the decrease in intensity and the increase in width of the diffraction peaks of samples grown with oxygen in the plasma suggest partial amorphization and grain refinement, which correlates with that observed by SEM in Fig. 1. According to the Scherrer equation, there is a relationship between the broadening of a peak in a diffraction pattern and the size of sub-micrometric crystallites. We have made use of such equation to obtain the mean crystal size of all samples grown between 0 and 70 % oxygen. The results are shown in Fig. 3. In all cases, the original data were fitted using a pseudo-Voigt curve. The gaussian contribution to this curve increases with the oxygen content, which suggests that there is more disorder as the oxygen content of the plasma increases (Table 1). The mean crystal size

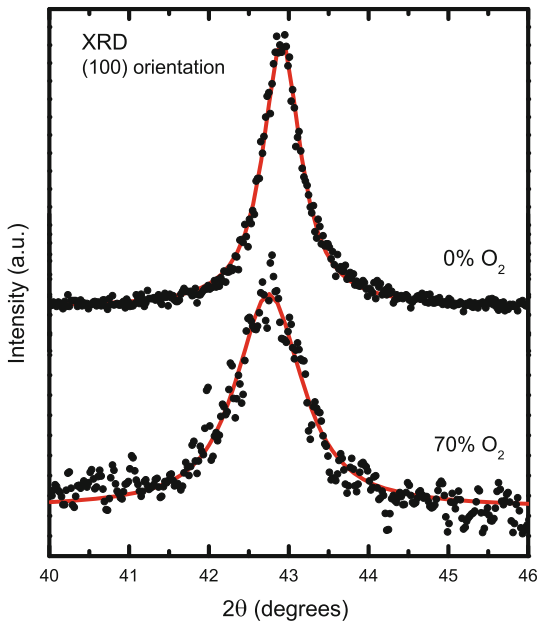

Fig. 2 X-ray diffraction patterns around the (100) peak of NiO films grown on Si with 0 and 60 % oxygen in the sputtering plasma, respectively. The *solid line* through the data points is the result of a least-squares fit using a pseudo-Voigt curve

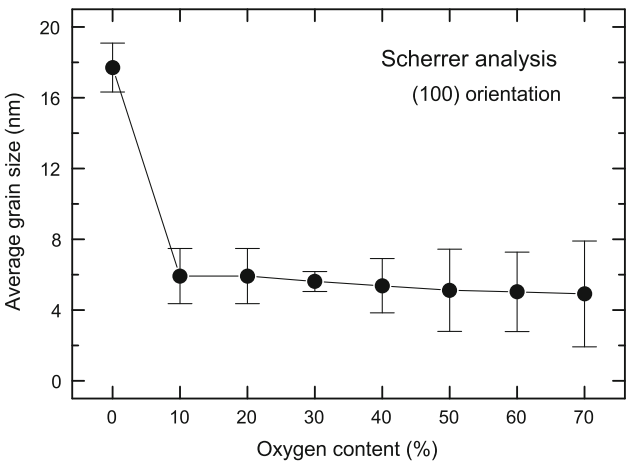

Fig. 3 Evolution of the average grain size of the nanocrystalline NiO films with the oxygen content of the plasma, as obtained from the XRD data using the Scherrer equation. The original data were previously fitted using a pseudo-Voigt curve

for the sample grown without oxygen is about 20 nm, which is in agreement with the microstructure shown in Fig. 1a and e. As some oxygen is added to the plasma, there is a sudden drop in the grain size, down to 6 nm for the 10 % sample. This crystal size is approximately kept constant when increasing the oxygen content in the plasma. According to these results, samples prepared in the presence of oxygen in the plasma present a considerable grain refinement.

Table 1 Width of the gaussian contribution to the pseudo-Voigt curves used in the fittings of the XRD data

Sample	Width (°)
0	0.45
10	0.60
20	0.66
30	0.68
40	0.76
50	0.82
60	0.86
70	0.88

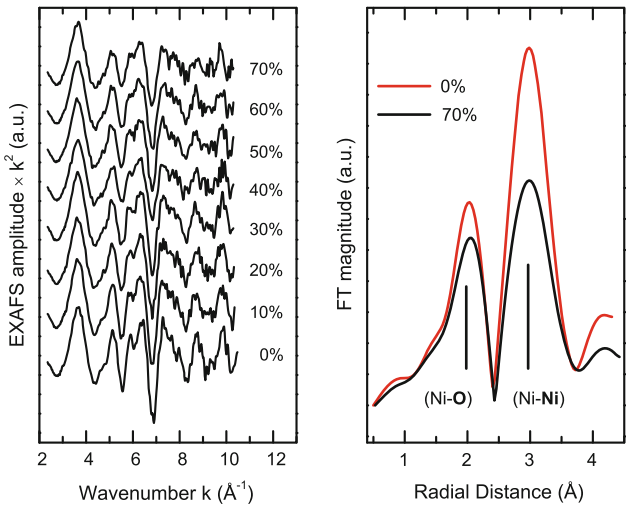

Fig. 4 *Left* EXAFS signal (k^2-weighed) of NiO films grown with different oxygen content in the sputtering plasma. *Right* module of the Fourier transform of the EXAFS signal for samples grown with 0 and 70 % oxygen. The central atom phase shift has been previously subtracted

Figure 4 shows the Ni K-edge k^2–weighed EXAFS signals for all samples (left), and the module of the Fourier transform for samples grown with 0 and 70 % oxygen in the plasma (right). The EXAFS signals have been obtained after removing the background using a cubic spline polynomial fitting, and normalizing the magnitude of the oscillations to the edge jump. In the determination of the Fourier transform, the central atom phase shift has been previously subtracted. The frequency of the oscillations of the EXAFS signal is very similar for all samples. On the other hand, the amplitude gradually decreases when the oxygen content of the plasma increases, especially at high k values. Such a decrease in the amplitude of the EXAFS oscillations can be caused by either a decrease of the coordination number or an increase of the structural disorder.

The peaks observed in the Fourier transform correspond to the first neighbor distance (Ni–O) and the second neighbor distance (Ni–Ni) around the absorber atom, respectively. The results of the fit analysis yield a first neighbor distance of 2.08 Å and a second neighbor distance of 2.96 Å for the sample grown with pure Ar. These values are slightly larger than those of bulk NiO [28]. In the case of the 70 % sample an expansion of about 1 % in the interatomic distances, as compared to the 0 % sample, is obtained from the fitting analysis, which confirms the lattice expansion observed by XRD. As it can be observed in Fig. 4, the intensity of both peaks for the 70 % sample is lower than for the 0 % sample. Such a decrease is related to the damping observed in the EXAFS signal when the oxygen content increases, and is thus related to a decrease of the coordination number and an increase of the disorder. NiO usually grows in a non-stoichiometric form as $Ni_{1-x}O$, i.e., with excess oxygen in the lattice. This results in the presence of a variable amount of Ni vacancies. As the oxygen content of the plasma increases, more oxygen incorporates to the lattice, generating a larger amount of Ni vacancies, as has been evidenced by X-ray absorption spectroscopy [27]. This is in agreement with the relative decrease of the FT peaks for the 70 % sample with respect to the 0 % sample, being larger for the second (Ni–Ni) peak than for the first one (Ni–O). Indeed, the FT curve of the sample grown with pure Ar could be fitted with a coordination number of 12 atoms for the second shell, which corresponds to the expected number of second neighbors in the NiO lattice. On the other hand, by increasing the oxygen content in the plasma the coordination number gradually decreases down to 11 atoms for the 70 % sample [22].

This deviation from stoichiometry can help to explain the grain refinement observed both by SEM and XRD. During the sputtering process, NiO clusters interact with the oxygen in the plasma along their path from the target to the substrate, incorporating some extra oxygen. When the clusters adsorb on the NiO coating already deposited on the substrate, diffusion occurs so they accommodate into the most energetically favorable position, which involves the growth of crystalline domains. However, the imperfections introduced in the lattice by the excess oxygen hinder the diffusion, so the size of the crystalline domains is smaller.

The intensity of the EXAFS peak corresponding to the first neighbor, i.e., to Ni–O bonds, also shows a decrease for the 70 % sample as compared to the 0 % sample. Since no changes in the coordination number are expected in this case, we associate this decrease with a larger degree of disorder in this sample. Indeed, both effects, an increase of the disorder and a decrease of the second neighbor coordination number, were needed to fit the EXAFS data. This large degree of disorder for samples grown with oxygen was already mentioned in the discussion of the XRD results, where an increase of the Gaussian contribution in

the pseudo-Voigt curve was needed in order to correctly fit the diffraction data.

The degree of disorder can be quantified from the analysis of the EXAFS data through a parameter, the Debye–Waller factor, usually denoted as σ^2. This parameter represents the mean-squared relative displacements and is a summation of the thermal disorder term and the crystal disorder [29]. Since all measurements were performed at room temperature, the thermal disorder affects equally all samples. Consequently, the changes observed in the Debye–Waller factor between the different samples can be assigned directly to structural disorder. Figure 5 shows the variation of the Debye–Waller factor, σ^2, for the second neighbor shell (Ni–Ni), as obtained from the EXAFS fit. The figure shows an increasing tendency of σ^2, which confirms that the oxygen content in the plasma increases the lattice disorder. An estimation of the errors of the fitting gives ± 0.002 Å^2 and 10 % for the σ^2 factor and the coordination number, respectively [30]. A disordered system like the present one does not allow a better precision, neither allows including more than the two first shells in the calculations due to the great sensitivity to disorder of the EXAFS technique.

The structural changes shown above are expected to have an influence on the electronic properties of the NiO films. NiO is a charge transfer oxide whose electronic structure gives rise to a complex Ni 2*p* spectrum with multiple peaks. In previous works we proposed that the shoulder at ≈ 1.5 eV from the main Ni $2p_{3/2}$ peak has two contributions: one coming from non-local screening and another one associated to surface effects, in which Ni ions are in pyramidal symmetry at the surface [12, 14]. Figure 6 shows XPS Ni $2p_{3/2}$ spectra of samples grown with 0 and 70 % oxygen in the plasma, respectively. The solid line through the data points is the result of a least-squares fit using Lorentz functions for the different components and a Shirley's background. The resulting curve was then convoluted with a Gaussian function to simulate the experimental resolution, which resulted to be 0.67 eV. The first component, at a binding energy of 854.5 eV, is assigned to $c3d^9\underline{L}$ transitions, where $\underline{L}$ denotes a hole at the ligand (oxygen) and *c* a Ni 2*p* core level hole [9]. The second component, at a binding energy of 856.1 eV, corresponds to the surface component, in which the apical oxygen on surface Ni ions is lacking [12, 14]. The third component, at a binding energy of 857.3 eV, is assigned to final states with non-local screening of the core hole [9]. The broad features centered at 861.5 and 867 eV correspond to $c3d^{10}\underline{L}^2$ and $c3d^8$ transitions, and are included in the fit for consistency. The ratio between the intensity of the main component and that of the non-local component was imposed to be the same for all samples. On the other hand, the intensity of the surface component can vary depending on the surface-to-volume ratio of the sample. Indeed, it can

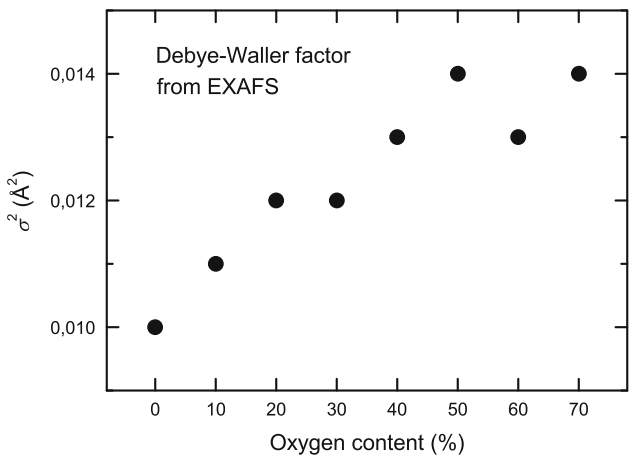

Fig. 5 Variation of the Debye–Waller factor, σ^2, for the second neighbor shell (Ni–Ni), as obtained from the EXAFS fit, with the oxygen content of the plasma. The uncertainty of the data is below 0.002 Å^2

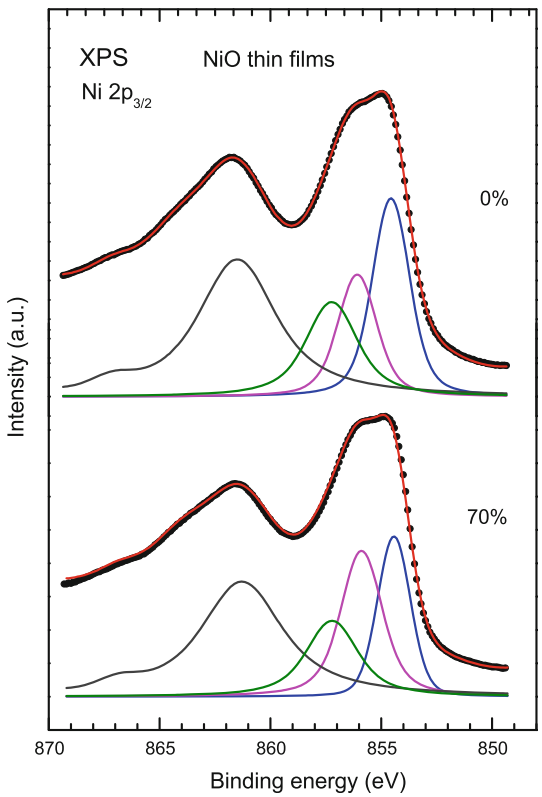

Fig. 6 XPS Ni $2p_{3/2}$ spectra of NiO films grown with 0 and 70 % oxygen in the plasma, respectively. The *solid line* through the data points is the result of a least-squares fit using Lorentz functions for the different components and a Shirley background. The resulting curve was then convoluted with a Gaussian function to simulate the experimental resolution. The different components are assigned to final states coming from surface or bulk atoms (see text)

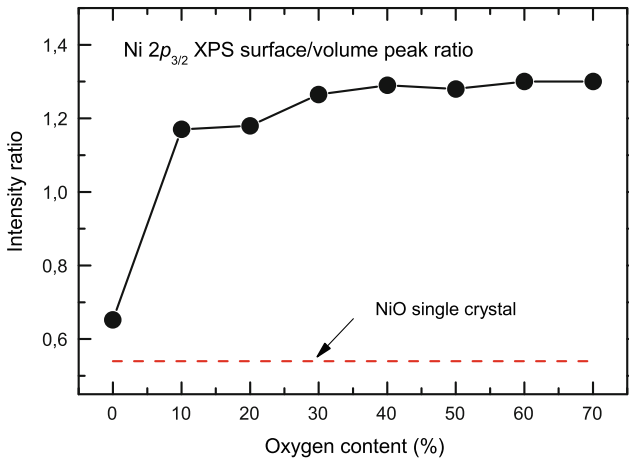

Fig. 7 Evolution of the XPS surface-to-volume peak ratio as a function of the oxygen content of the plasma. The *horizontal dashed line* gives the value corresponding to NiO single crystal, from Ref. [14]

be clearly observed in Fig. 6 that the surface component for the sample grown with 70 % oxygen in the plasma is relatively more intense than for the sample grown with pure Ar. As it has been shown above, the grain size of the NiO films decreases upon oxygen addition to the plasma, which is consistent with a higher surface-to-volume ratio for samples grown with oxygen.

The ratio between the surface peak and the main bulk peak of the XPS Ni $2p_{3/2}$ spectra can give information on the relative signal coming from the surface, which should be correlated with the crystallite size. Even though this parameter does not seem to depend on the oxygen content in the plasma during growth, as seen in Fig. 3, but just on the presence or absence of oxygen, we have fitted all XPS spectra for the different oxygen content values. Figure 7 shows the evolution of the XPS surface-to-volume peak ratio as a function of the oxygen content of the plasma. The value obtained for the 0 % sample is ≈ 0.65, higher than the value of 0.54 expected for single crystal NiO [14]. By adding 10 % oxygen to the plasma, a sudden increase in this ratio is observed, to a value close to 1.2, which indicates a larger contribution of the surface. For higher oxygen content, the surface-to-volume ratio remains approximately constant. This behavior correlates very well with the reduction in crystal size shown in Fig. 3, in which a sudden drop in the grain size was observed when going from 0 to 10 %, and afterwards it remained almost constant. This result provides an excellent example of the correlation between electronic and structural properties in this material. It also confirms that the intensity variations of the 1.5 eV shoulder in the Ni $2p_{3/2}$ XPS spectra of NiO can be associated with surface effects.

Conclusions

NiO nanostructured thin films have been grown by off-axis reactive RF magnetron sputtering from a NiO target with a mixed O_2-Ar plasma composition. The oxygen addition during the sputtering process modifies the morphology of the thin films by decreasing the grain size, as was observed by SEM. A grain size reduction from 20 to 5 nm approximately was confirmed by XRD after performing a Scherrer analysis, and is in accordance with the SEM observations. The lower intensity of the diffraction peaks for the samples grown with oxygen suggests partial lattice disorder. Additionally, a slight lattice expansion for samples grown with oxygen in the plasma was observed. The EXAFS results confirm this lattice expansion, as well as the lattice disorder with the oxygen content of the plasma, as quantified by the Debye–Waller factor. The observed structural changes induced by the addition of oxygen to the sputtering plasma during deposition have an influence on the electronic properties of the NiO films. The XPS Ni $2p_{3/2}$ spectra of samples grown with oxygen show a larger intensity of the peak assigned to surface atoms that can be associated with the grain refinement observed by XRD and EXAFS. The behavior of the surface peak intensity in the presence or absence of oxygen content in the plasma correlates very will with that observed on the average grain size obtained by XRD.

Acknowledgements This work has been supported by the Spanish MICINN, under projects ENE2010-21198-C04-04, MAT2011-27573-C04-04, and CSD2008-0023. We acknowledge the European Synchrotron Radiation Facility (ESRF) and the SpLine CRG beamline staff for provision of synchrotron radiation and for assistance during X-ray absorption experiments.

References

1. Liu KC, Anderson MA (1996) Porous nickel oxide/nickel films for electrochemical capacitors. J Electrochem Soc 143(1): 124–130
2. Nam KW, Yoon WS, Kim KB (2002) X-ray absorption spectroscopy studies of nickel oxide thin film electrodes for supercapacitors. Electrochim Acta 47(19):3201–3209
3. Estrada W, Andersson AM, Granqvist CG (1988) Electrochromic nickel-oxide-based coatings made by reactive dc magnetron sputtering: preparation and optical properties. J Appl Phys 64(7):3678–3683
4. Hotovy I, Huran J, Spiess L, Hascik S, Rehacek V (1999) Preparation of nickel oxide thin films for gas sensors applications. Sensors Actuators B 57:147–152
5. Nuli YN, Zhao SL, Qin QZ (2003) Nanocrystalline tin oxides and nickel oxide film anodes for Li-ion batteries. J Power Sources 114(1):113–120
6. Choudhary VR, Uphade BS, Mamman AS (1998) Simultaneous steam and CO_2 reforming of methane to syngas over NiO/MgO/SA-5205 in presence and absence of oxygen. Appl Catal A 168(1):33–46

7. Dissanayake D, Rosynek MP, Kharas KC, Lunsford JH (1991) Partial oxidation of methane to carbon monoxide and hydrogen over a Ni/Al_2O_3 catalyst. J Catal 132(1):117–127
8. Fujimori A, Minami F, Sugano S (1984) Multielectron satellites and spin polarization in photoemission from Ni compounds. Phys Rev B 29(9):5225–5227
9. van Veenendaal MA, Sawatzky GA (1993) Nonlocal screening effects in 2p x-ray photoemission spectroscopy core-level line shapes of transition metal compounds. Phys Rev Lett 70(16): 2459–2462
10. Taguchi M, Matsunami M, Ishida Y, Eguchi R, Chainani A, Takata Y, Yabashi M, Tamasaku K, Nishino Y, Ishikawa T, Senba Y, Ohashi H, Shin S (2008) Revisiting the valence-band and core-level photoemission spectra of NiO. Phys Rev Lett 100(20):206401
11. Soriano L, Preda I, Gutiérrez A, Palacín S, Abbate M, Vollmer A (2007) Surface effects in the Ni 2p X-ray photoemission spectra of NiO. Phys Rev B 75(23):233417
12. Mossanek RJO, Preda I, Abbate M, Rubio-Zuazo J, Castro GR, Vollmer A, Gutiérrez A, Soriano L (2011) Investigation of surface and non-local screening effects in the Ni 2p core level photoemission spectra of NiO. Chem Phys Lett 501(4-6):437–441
13. Palacín S, Gutiérrez A, Preda I, Hernández-Velez M, Sanz R, Jiménez JA, Soriano L (2007) Core-level electronic properties of nanostructured NiO coatings. Appl Surf Sci 254(1):278–280
14. Preda I, Mossanek RJO, Abbate M, Álvarez L, Méndez J, Gutiérrez A, Soriano L (2012) Surface contributions to the XPS spectra of nanostructured NiO deposited on HOPG. Surf Sci 606(17–18):1426–1430
15. Han SY, Lee DH, Chang YJ, Ryu SO, Lee TJ, Chang CH (2006) The growth mechanism of nickel oxide thin films by room-temperature chemical bath deposition. J Electrochem Soc 153(6):C382–C386
16. Fujii E, Tomozawa A, Torii H, Takayama R (1996) Preferred orientations of NiO films prepared by plasma-enhanced metal-organic chemical vapor deposition. Jpn J Appl Phys 2(35):L328–L330
17. Patil PS, Kadam LD (2002) Preparation and characterization of spray pyrolyzed nickel oxide (NiO) thin films. Appl Surf Sci 199(1):211–221
18. Jang WL, Lu YM, Hwang WS, Hsiung TL, Wang HP (2009) Point defects in sputtered NiO films. Appl Phys Lett 94(6):062103
19. Ryu HW, Choi GP, Lee WS, Park JS (2004) Preferred orientations of NiO thin films prepared by RF magnetron sputtering. J Mater Sci 39(13):4375–4377
20. Nandy S, Saha B, Mitra MK, Chattopadhyay KK (2007) Effect of oxygen partial pressure on the electrical and optical properties of highly (200) oriented *p*-type $Ni_{1-x}O$ films by DC sputtering. J. Mater. Sci. 42(14):5766–5772
21. Thornton JA (1986) The microstructure of sputter-deposited coatings. J Vac Sci Technol A 4(6):3059–3065
22. Gutiérrez A, Domínguez-Cañizares G, Jiménez JA, Preda I, Díaz-Fernández D, Jiménez-Villacorta F, Castro GR, Chaboy J, Soriano L (2013) Hexagonally-arranged-nanoporous and continuous NiO films with varying electrical conductivity. Appl Surf Sci 276:832–837
23. Sayers DE, Bunkler BA (1988) Data analysis. In: Koningsberger DC, Prins R (eds) X-ray absorption: principles, applications, and techniques of EXAFS, SEXAFS, and XANES. Wiley, New York, pp. 211–256
24. Klementev KV (2000) Package VIPER (visual processing in EXAFS researches) for windows. Nucl Instrum Methods A 448(1): 299–301
25. Klementev KV (2001) Extraction of the fine structure from x-ray absorption spectra. J Phys D 34(2):209–217
26. Chen SC, Kuo TY, Sun TH (2010) Microstructures, electrical and optical properties of non-stoichiometric *p*-type nickel oxide films by radio frequency reactive sputtering. Surf Coat Technol 205: S236–S240
27. Mossanek RJO, Domínguez-Cañizares G, Gutiérrez A, Abbate M, Díaz-Fernández D, Soriano L (2013) Effects of Ni vacancies and crystallite size on the O 1s and Ni 2p X-ray absorption spectra of nanocrystalline NiO. J Phys Condens Matter 25(49):495506
28. Anspoks A, Kuzmin A (2011) Interpretation of the Ni K-edge EXAFS in nanocrystalline nickel oxide using molecular dynamics simulations. J Non-Cryst Solids 357(14):2604–2610
29. Theye ML, Gheorghiu A, Launois H (1980) Investigation of disorder effects in amorphous GaAs and GaP by EXAFS. J Phys C 13(36):6569–6584
30. Corrias A, Mountjoy G, Piccaluga G, Solinas S (1999) An X-ray absorption spectroscopy study of the Ni K edge in $NiO-SiO_2$ nanocomposite materials prepared by the Sol–Gel method. J Phys Chem B 103(46):10081–10086